PHYSICAL REVIEW B VOLUME 25, NUMBER 12 15 JUNE 1982

Oxygen K near-edge fine structure: An electron-energy-loss investigation with comparisons to new theory for selected $3d$ transition-metal oxides

L. A. Grunes and R. D. Leapman*
School of Applied and Engineering Physics and Materials Science Center, Cornell University, Ithaca, New York 14853

C. N. Wilker and R. Hoffmann
Department of Chemistry and Materials Science Center, Cornell University, Ithaca, New York 14853

A. B. Kunz
Department of Physics and Materials Research Laboratory, University of Illinois, Urbana, Illinois 61801

(Received 28 December 1981; revised manuscript received 10 March 1982)

Excitations of the oxygen $1s$ subshell in selected $3d$ transition-metal oxides have been studied by inelastic scattering of 75-keV electrons. Striking variations in the near-edge fine structure are reported and an interpretation is developed based on an empirical molecular orbital energy-level model. We compare our observed fine structure with that evinced in the metal K and L_3 edges in these same oxides. While the molecular-orbital model seems adequate for interpreting the spectra of TiO_2, it fails for at least some of the oxides studied. For example, in the case of NiO, a self-consistent Hartree-Fock computation for the oxygen $1s$ excitation spectrum gives results showing that the near-edge structure is not adequately described by the unoccupied density of states of the solid before core-hole excitation. Instead, the initial spectral peaks are shown to be core excitons. However, for TiO_2, a tight-binding extended Hückel calculation neglecting the core hole yields a density of states that displays peaks in good agreement with the experimental data. Speculations on the origin of the difference between the spectra of NiO and TiO_2 are offered.

I. INTRODUCTION

While much progress has been made in interpreting the weak fine-structure oscillations extending to several hundred eV past x-ray absorption[1–5] or electron-energy-loss[6,7] core edges, the stronger intensity variations occurring within the first ~ 30 eV above onset are less well understood. The extended x-ray absorption fine structure (EXAFS) has been shown by Stern and co-workers[1–5] to be directly related to the atomic radial distribution function around the excited atom. EXAFS analysis has become a standard structural probe for complex biological and other systems. By contrast, interpretation of the near-edge absorption fine structure of compounds has been largely qualitative and often lacking theoretical support. Recently, molecular cluster calculations have achieved some success in predicting K-edge structure in various gases.[8,9] The observed near-edge features have been shown to be related to the unoccupied electronic molecular-energy levels as modified by the creation of a core hole. In condensed matter additional band, excitonic, and magnetic effects can come into play, and calculations for core edges in nonmetallic solids are virtually nonexistent.

The $3d$ transition-metal oxides display striking magnetic and electronic properties of technological utility and the interpretation of their near-edge structure therefore presents an interesting and important problem. In this study, we (L.A.G. and R.D.L.) report gross variations in the oxygen K near-edge structure between various $3d$ transition-metal oxides as measured by electron-energy-loss spectroscopy (EELS). We then present an initial interpretation of the data based upon an empirical symmetry-determined molecular-orbital (MO) picture using a comparison of the near-edge structure found on the metal K and L edges in these same oxides. Finding this approach to be in some cases inadequate, we then turn to band calculations. A tight-binding extended Hückel band structure for

TiO_2 is computed (C.N.W. and R.H.) and shows essential agreement with the molecular-orbital interpretation of the data. Further, the band gap between the valence and conduction bands and also the peak separations in the conduction-band density of states agree well with experiment. However, this calculation omits excitonic and magnetic effects. While TiO_2 is nonmagnetic, NiO is an antiferromagnet and hence presents a much more difficult problem. Accordingly, tight-binding calculations are of little use in predicting the core-excitation spectra. An *ab initio* spin-polarized calculation has been completed for the band structure of antiferromagnetic NiO (A.B.K.), and the corresponding single-electron oxygen K-edge transition probability calculated with neglect of core-hole effects. However, the allowed core exciton series has been computed so that the combined band and exciton results can be compared with the observed oxygen K-edge fine structure. We find our prior assumption that the near-edge structure is related to the unoccupied density of states of the initial solid (before core-hole excitation) to be invalid. Rather, the threshold spectral peaks are shown to be core excitons. The presence of excitons explains the lack of correlation between the peaks of the near-edge structure for different atoms in the same solid.

Before proceeding to the experimental results, we must first explain the electronic transition probabilities whose variations give rise to the EELS and x-ray absorption spectra (XAS). In the case of XAS, dipole selection rules apply ($\Delta l=\pm 1$); for excitation of the oxygen K ($1s$) level, the final state must have p symmetry. The photoabsorption cross section is written within the single-electron model and the first Born approximation in terms of a dipole matrix element between an initial core state $|i\rangle$ and final state $|f\rangle$ as[10]

$$\sigma_{\text{abs}}(E)=\frac{4\pi^2e^2}{\hbar c}E\,|\langle f|\vec{e}\cdot\vec{r}|i\rangle|^2\,, \tag{1}$$

where E is the photon energy and $\vec{e}$ is a unit vector in the direction of the electric field. The cross section for inelastic electron scattering in a transition between two similar states is given by[11]

$$\frac{d^2\sigma(E,q)}{dE\,dq}=\frac{8\pi e^4}{\hbar^2v^2}\frac{1}{q^3}\,|\langle f|\exp(i\vec{q}\cdot\vec{r})|i\rangle|^2\,, \tag{2}$$

where $\vec{q}$ is the momentum transfer, E is the energy transfer, and v is the incident electron velocity. Equation (2) can be expanded as

$$\frac{d^2\sigma(E,q)}{dE\,dq}=\frac{8\pi e^4}{\hbar^2v^2}\frac{1}{q^3}\,|\langle f|1+iq(\vec{\epsilon}_q\cdot\vec{r})-q^2(\vec{\epsilon}_q\cdot\vec{r})^2+\cdots|i\rangle|^2\,, \tag{3}$$

where $\vec{\epsilon}_q$, a unit vector in the direction of $\vec{q}$, plays the role of the electric-field-polarization vector $\vec{e}$ in the case of x-ray absorption. Within the small scattering angle approximation, which requires the momentum transfer $q\ll r_c^{-1}$, where r_c is the core orbital radius, the matrix element in Eq. (3) can be reduced to $\langle f|\epsilon_q\cdot r|\rangle$ and the quadrupole and higher-order terms can be neglected.[12] The differential cross section is then of the same form as that in Eq. (1) so in this limit we expect a complete correspondence between energy-loss and photoabsorption data, as is well known (e.g., Ref. 13).

The measured core-edge intensity may be decomposed into the product of a matrix element factor $P(E)$ and a projected density of states $N(E)$ with appropriate symmetry[14,15]:

$$I(E)\propto P(E)N(E)\,. \tag{4}$$

Therefore, the fine structure near the core-edge onset is expected to reflect the unoccupied density of states in the conduction band only if the matrix-element factor is slowly varying in that energy region. Calculations for the K and L edges in the $3d$ transition metals indicate that this is indeed the case.[15,16]

II. EXPERIMENTAL

A. Instrumentation

The experimental system for recording the spectra has been described previously.[17] This consists of an HU11A transmission electron microscope combined with a retarding field Wien filter spectrometer. The electron microscope is used in the selected area diffraction mode to form a 4-μm probe of 75-keV electrons on the specimen with a beam convergence of less than 10^{-3} rad. An entrance slit to the Wien filter spectrometer selects electrons according to their scattering angle and the spectrometer disperses them in a direction perpendicular to the slit. Spectra are recorded by

scanning the energy-loss intensity across an apertured scintillator and by counting the single pulses derived from a photomultiplier. In the present experiments the aperture subtends a scattering angle of approximately ± 2 mrad corresponding to momentum transfers up to 0.3 Å^{-1} for which the dipole approximation (above) holds. Digital scans of 0–200 eV are controlled by a microcomputer which also stores the spectrum.[18,19] After acquisition, the data is uploaded to a PDP11/20 computer for processing. Since the spectrometer has a resolution of <0.1 eV, the energy resolution of the measured spectra (1 or 2 eV) is determined mainly by the thermal spread of the incident beam. Absolute measurement of the energy losses is accurate to about 0.5 eV.

B. Samples

Thin polycrystalline metallic films were first prepared by electron-beam evaporation in an ion-pumped high-vacuum system at a base pressure of about 2×10^{-8} Torr. Film thicknesses of 15-nm titanium, 15-nm chromium, 26-nm iron, 9-nm nickel, and 24-nm copper were measured using a quartz-crystal thickness monitor situated near the substrate, which was the (100) face of a cleaved rock-salt crystal. All the metal films obtained in this way were polycrystalline with a grain size between 5 and 100 nm. They were floated off in ethanol and supported on 3-mm-diam copper grids (400 mesh per inch). Oxide films were then prepared by taking metal films already supported on grids and heating them in air. The oxides were characterized by means of electron diffraction and imaging in the microscope before data collection. The polycrystalline ring diffraction patterns were matched to the *d* spacings as given by the x-ray Powder Diffraction File,[20] enabling us to determine the oxidation state of the films. In each case the diffraction patterns contained only those rings expected from one oxide; no evidence for residual metal or different oxidation states was found. Grain sizes for the oxides of 100 to 1000 nm were larger than for the metal films prior to oxidation.

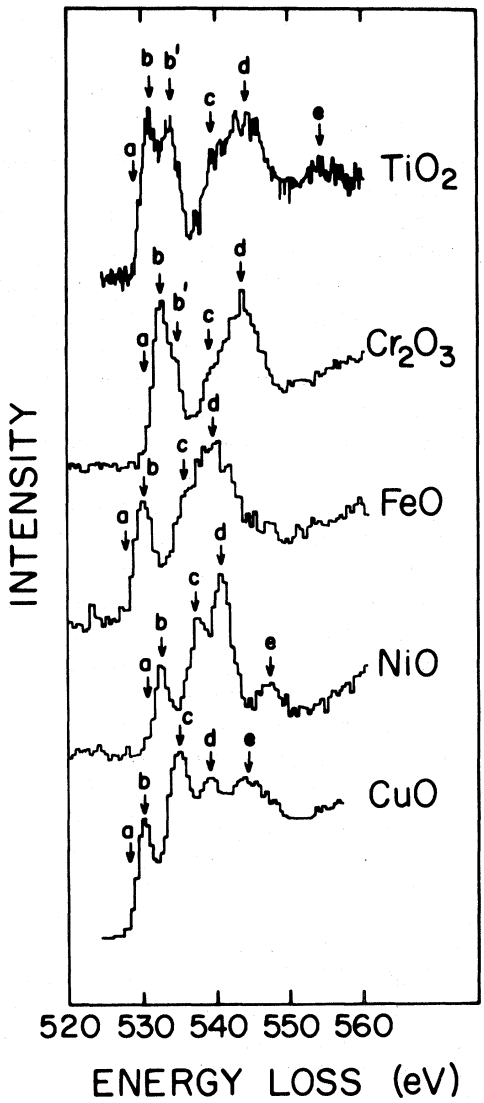

FIG. 1. O *K*-shell excitation edges measured by EELS for selected 3*d* transition-metal oxides.

TABLE I. Energy-loss values for the O *K*-edge onset (a) and near-edge fine structure (peaks *b*–*e*) shown in Fig. 1.

Material	*a*	*b*	*b'*	*c*	*d*	*e*
TiO_2	530.0	531.0	533.5	539.5	543.5	554.0
Cr_2O_3	531.0	532.5	534.5	539.0	543.5	
FeO	529.0	530.0		536.0	539.0	
NiO	531.0	532.5		537.5	540.5	547.0
CuO	529.0	530.0		535.0	539.0	544.0

C. Results

Oxygen K (OK) edges were recorded by electron-energy-loss spectroscopy in transmission at small scattering angles so that the dipole approximation (above) holds. Figure 1 presents the experimental results for TiO_2, Cr_2O_3, FeO, NiO, and CuO recorded with a resolution of $\sim 1\frac{1}{2}$ eV. The background has been subtracted off by fitting to an inverse power law AE^{-r} where E is the transmitted electron energy loss. Chemical shifts in the energy at onset (a) and differences in fine-structure peaks ($b-e$) are clearly visible; the various energies $a-e$ are listed in Table I. Charge transfer from the metal to oxygen atoms, along with excitonic effects and variations in the width of the band gap, are all expected to influence the threshold energy. Core excitons and maxima in the unoccupied p density of states (DOS) contribute to the multipeaked structure which is characteristic of the oxide. This structure varies between the oxides shown despite the fact that in all cases the metal atom is octahedrally coordinated to its six nearest-neighbor oxygens, and hence the local arrangement of atoms is quite similar. We note that these fine-structure peaks must be characteristic of the solid since atomic effects are unimportant. (The K-shell photoionization cross section in atomic oxygen shows only a sharp rise at onset followed by a long decaying tail.[21])

A trend visible in the spectra is a narrowing of the combined width of the initial peaks (b,b') as we go across the 3d period from TiO_2 to CuO. We have observed this same decreasing trend in the metal L_3 spectra of these oxides and have discussed this effect in terms of the filling of the metal 3d bands with increasing atomic number.[22] In a molecular-orbital picture, the d orbitals from the metal atoms mix with the p orbitals from the oxygen atoms. Hence, $1s \rightarrow p$ transitions (OK edge) might be expected to reflect to some extent the d density of states around the metal atoms as measured by the L_{23} edges. Table II shows these two sets of measured widths, after correction for the finite experimental energy resolution of the spectra (corrected width $=[(\text{measured width})^2-(\text{energy resolution})^2]^{1/2}$). These values support in part the interpretation that this decreasing trend in the combined width of the oxide peaks (b,b') is also a manifestation of the metal d-band filling, and we shall discuss this later.

TABLE II. Measured full widths at half maximum (FWHM) in eV corrected for finite experimental energy resolution.

Material	OK (b,b') FWHM	Metal L_3 peak FWHM
TiO_2	5.6±0.3	4.0±0.3
Cr_2O_3	3.3	3.2
FeO	3.1	3.2
NiO	2.9	1.2
CuO	2.6	1.3

The 3d transition-metal oxide OK edges have been previously measured by various experimental techniques and we find the available data to be consistent with ours. Fischer has measured OK edges in TiO_2 (Ref. 23) and Cr_2O_3 (Ref. 24) by using two x-ray emission spectra obtained with different incident x-ray energy beams. Since the more energetic beam penetrates deeper into the sample, the logarithm of the ratio of these two emission spectra yields a "self-absorption" spectrum which should be equivalent to an x-ray absorption experiment. Fischer's spectra extend only to the energy region (first ~ 5 eV) where the emission and absorption spectra overlap. He observes our peaks b and b' in both TiO_2 and Cr_2O_3, although his intensities differ from ours. This is not surprising, however, since self-absorption is not a direct-measurement technique and is probably nonlinear in intensity.

The OK edge in NiO has been recorded by measuring the total electron yield from a NiO film while it is bombarded by a monochromated synchrotron x-radiation beam by Stöhr *et al.*[25] This "total electron yield spectroscopy" also is expected to be equivalent to an x-ray absorption measurement. Since practical problems are encountered in monochromating synchroton radiation in this energy range (~ 500 eV), the energy resolution of the data cited is only ~ 5 eV. Hence our peaks $b-e$ are blurred in their spectrum into one broad peak with two small shoulders at energies corresponding to our peaks b and e. These authors were more concerned with an EXAFS analysis which requires good counting statistics rather than high-energy resolution. The radial distribution function which they obtain by Fourier transforming their data agrees well with the result we have obtained from a more extended energy-loss OK spectrum.[6]

3d transition-metal-oxide OK edges have also been reported by several authors using appearance potential spectroscopy (APS). In this method, the total x-radiation emitted by the sample is measured as a function of the energy of the bombarding electron beam. A small increase in x-ray emission is observed when the incident electron energy reaches

a core electron ionization threshold. Because the incident and excited core electrons both make transitions to states near the Fermi level, and because a derivative signal is recorded, the APS spectral intensity is proportional to the derivative of the self-convolution of the final density of states. However, these spectra can closely resemble the DOS itself, as illustrated by Nagel *et al.*[26] Since the incident electron energy for the APS measurement of the OK level is only ~ 500 eV, the bombarding beam penetrates only to <20 Å, and hence APS is essentially a surface probe. It is therefore somewhat surprising and interesting that APS results from oxidized surfaces of Ti, Cr, Fe, and Ni (Refs. 27–29) all display fine structure closely resembling that of our EELS transmission spectra through ~ 200-Å films, which should show mainly the effects of the bulk component of the DOS.

In summary, previous OK fine-structure measurements are consistent with our EELS results, although the various nonlinearities resulting from the indirect experimental procedures employed produce some variation in the spectral shapes and peak intensities.

III. DISCUSSION AND THEORY

A. Molecular-orbital picture

Previous attempts to interpret the core near-edge fine structure in the 3d transition-metal oxides have invoked a symmetry-determined molecular-orbital model for a cluster consisting of a metal atom surrounded by its oxygen nearest neighbors. In the oxides whose spectra are shown in Fig. 1, each metal atom is octahedrally coordinated to its six nearest-neighbor oxygen atoms (four in the basal plane and one each above and below). By considering the symmetry of the metal-ligand atomic-orbital pairings, a molecular-orbital energy-level hierarchy is deduced. Figure 2 shows[30] such an energy-level diagram with valence electron occupancies for the $(TiO_6)^{8-}$ cluster representing the environment around Ti in TiO_2. The level spacings are as yet unknown, since symmetry considerations cannot yield quantitative energies. This same level hierarchy also applies to the octahedral metal-oxygen clusters found in the rest of the oxides listed in Table I, the only difference being the increase in the number of filled orbitals as the metal-ion atomic number increases.

In the case of TiO_2, we see that the 48 valence electrons completely fill the π and σ bonding orbitals containing mostly oxygen 2p character, leaving

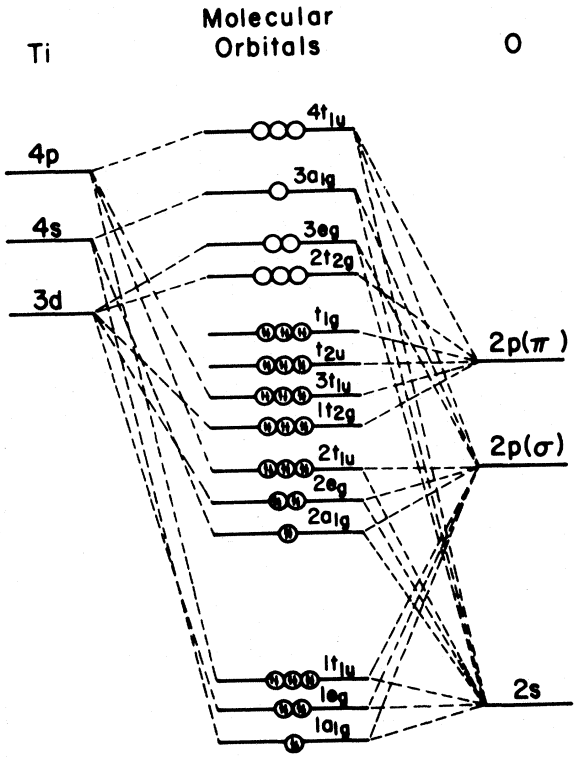

FIG. 2. MO energy-level diagram for $(TiO_6)^{8-}$, representing the environment around Ti in TiO_2 (Ref. 30).

unfilled the antibonding orbitals $2t_{2g}(d_{\pi^*})$ and $3e_g(d_{\sigma^*})$ containing mostly Ti d character. (Sketches of these two sets of orbitals appear in Fig. 7.) Accepting this picture, one can now measure the energy-level spacings directly from the near-edge fine structure on the various core edges. Invoking the dipole approximation $\Delta l = \pm 1$ (see above) appropriate to XAS or EELS at small angles, we consider the OK ($1s \rightarrow p$ states around O atom), TiK ($1s \rightarrow p$ states around Ti atom), and TiL_3 ($2p_{3/2} \rightarrow$ mostly d states around Ti atom) core excitations. These three edges are shown in Fig. 3 for the case of TiO_2. The TiK x-ray absorption and emission data (positive and negative energies, respectively) are taken from Ref. 30. [While the OK (530 eV) and TiL_3 (459 eV) edges lie at energies conveniently measured by EELS, the decrease of the electron cross section with energy loss makes x-ray absorption a superior measurement technique for the TiK edge at 4964 eV.] As is apparent from Fig. 3, the spacings of the first two peaks in all three edges are identical. This observation supports the interpretation that the final states in all three transitions are in fact the same, namely, the $2t_{2g}$ and $3e_g$ antibonding orbitals. Since these two orbitals are combinations of the Ti

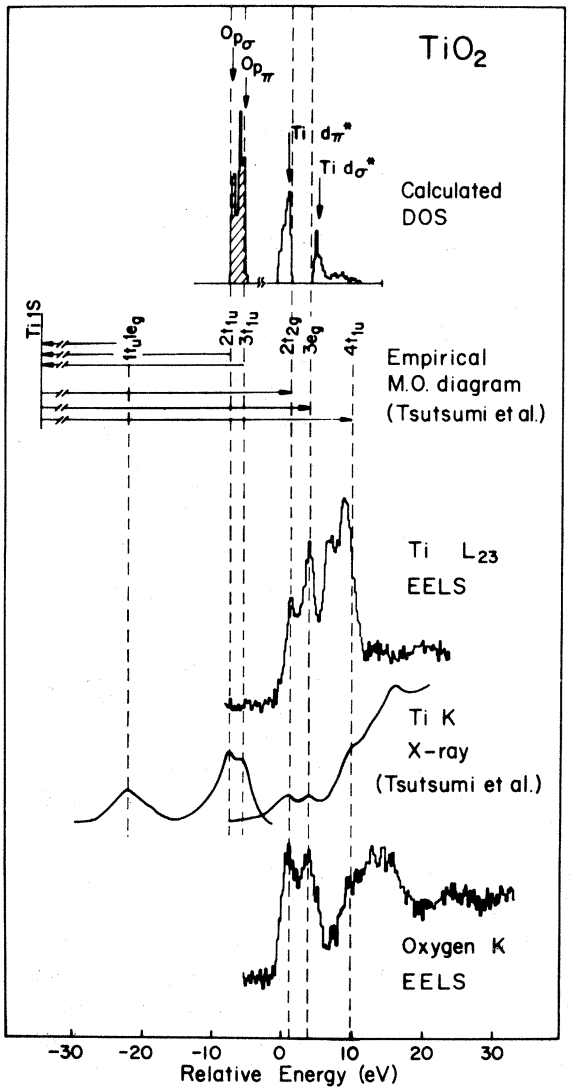

FIG. 3. Fine-structure peaks in the Ti L_{23}, Ti K (Ref. 30), and O K edges are aligned to construct an empirical MO level diagram. The energy-level spacings are in good agreement with peaks in our calculated conduction-band DOS.

3d orbitals and O 2p orbitals probed by the Ti L_{23} and O K edge, respectively, we expect the strong transition strengths observed, while the relative weakness of the peaks in the Ti K edge is explained by the absence of p character in these molecular orbitals near the metal atom.

In Fig. 3, the Ti L_3-edge fine structure is obscured from 6 eV above onset by the Ti L_2 edge, which also displays the $2t_{2g}-3e_g$ final-state splitting. Further fine structure past the Ti K and O K edges is attributed to transitions to higher levels, although the alignment of these peaks is less obvious.

In TiO_2 and Cr_2O_3, both the $2t_{2g}$ and $3e_g$ levels are expected to be at least partially unoccupied, while in FeO, NiO, and CuO only the $3e_g$ level remains unfilled. Consistent with this molecular orbital picture, the initial peak is split into two components, b and b' in TiO_2 and Cr_2O_3 O K edges (Fig. 1), while only one peak (b) is visible in FeO, NiO, and CuO, narrowing in width as we go across the period as expected from the filling of the $3e_g$-band broadened level.

The technique just illustrated for TiO_2 of using multiple x-ray absorption edges and aligning them with each other to produce an empirical set of molecular-orbital energy-level spacings is due to Fischer, who applied it to numerous Ti, V, and Cr oxides including TiO_2 (Ref. 23) and Cr_2O_3.[24] In Table III(a) we compare our empirical MO energy-level spacings with those of Fischer[23] (deduced by lining up three absorption edges as in Fig. 3) and of Tsutsumi *et al.*[30] (deduced from the Ti K edge shown in Fig. 3). These authors disagree over the assignment of the third and fourth peaks above onset. Tsutsumi argues that the transition $\mathrm{Ti}-1s\rightarrow 3a_{1g}$ is dipole forbidden and therefore should not appear in his Ti K absorption spectrum. Hence he assigns the third and fourth spectral peaks as transitions to the $4t_{1u}$ and $5t_{1u}$ levels. However, the appearance of the third peak (c) in our O K data in which the transition to $3a_{1g}$ is dipole allowed at the same relative energy as the third peak in the Ti K data tends to support Fischer's assignment scheme, which we adopt in Table III(a).

Using self-absorption, Fischer was able to measure only the first ~ 5 eV of the Ti L_3 and O K edges (see above). Hence only the $2t_{2g}$ and $3e_g$ peaks appear in these two spectra and also in the more extended Ti K-edge data of Albrecht *et al.*[31] which Fischer analyzed. Our extended O K-edge spectrum yields a relative $3a_{1g}$ energy in good agreement with both Fischer's and Tsutsumi's Ti K-edge peak energies, while our $4t_{1u}$ level is at a lower energy than either the weak shoulder (13.3 eV) or the more pronounced hump (15.3 eV) which are evinced in Tsutsumi's Ti K edge (Fig. 3).

Table III(b) compares our MO spacings for Cr_2O_3 with Fischer's. Again, only the initial $2t_{2g}$ and $3e_g$ peaks appear in Fisher's O K and metal-L_3 spectra, while the $3a_{1g}$ and $4t_{1u}$ assignments are deduced solely from a Cr K-edge measurement by Menshikov *et al.*[32] The agreement between our two sets of results is not as close as for TiO_2.

The molecular-orbital model for the metal-plus-

TABLE III. Comparison of empirical energies in eV of the unoccupied MO's relative to the lowest unfilled ($2t_{2g}$) level for TiO_2 (a) and Cr_2O_3 (b) as deduced from core-edge peak spacings.

		(a) $2t_{2g}$	$3e_g$	$3a_{1g}$	$4t_{1u}$
TiO_2	Present study	0	2.5	8.5	12.5
	Fischer (Ref. 23)	0	2.1	8.4	15.8
	Tsutsumi *et al.* (Ref. 30)	0	3.0	8.8	13.3 15.5
		(b) $2t_{2g}$	$3e_g$	$3a_{1g}$	$4t_{1u}$
Cr_2O_3	Present study	0	2.0	6.5	11.0
	Fischer (Ref. 24)	0	2.6	9.0	15.0

oxygen nearest-neighbors cluster discussed above has been invoked by numerous authors (e.g., Refs. 33–36) for interpreting metal–K-edge absorption spectra of various $3d$ transition-metal oxides. However, since only the metal K edge is measured, no multiple core-edge self-consistency check of the kind illustrated in Fig. 3 is ever applied. This apparent oversight may be due to the relative difficulty of obtaining x-ray absorption spectra in the vacuum ultraviolet energy region (450–950 eV) where the metal L_3 and O K edges lie. Synchrotron radiation monochromators in this spectral region are still in the development stage.[25] Also, preparation of uniform specimens with an optimized thickness of $t = 1/u \sim$ few tenths of a micron is also a problem, and we have discussed both these topics elsewhere.[22] In any case, when we compare the O K, metal K (Ref. 37), and metal L_3 (Ref. 22) fine structures in the rest of the oxides listed in Table I, we find three distinct sets of fine-structure peaks whose spacings do not match at all. This is illustrated for the case of CuO in Fig. 4. The intense L_3 peak shown in the top curve represents transitions to states of high d density around the Cu atom,[22] and as for the case of TiO_2, we line this peak up with the first fine-structure peaks in the O K edge (transition to p DOS around O atom, see Fig. 2), and in the Cu K edge (transitions to p DOS around Cu atom). As is evident from Fig. 4, the dashed lines drawn through the O K peaks cleanly miss the marked secondary maxima in the Cu L_3 edge, while the match to the small bumps in the Cu K x-ray edge is unconvincing. Nor does realigning the three edges in a different scheme improve things. We conclude that something is fundamentally wrong with the simple MO model for interpreting these spectra which seemed to work so well in the case of TiO_2.

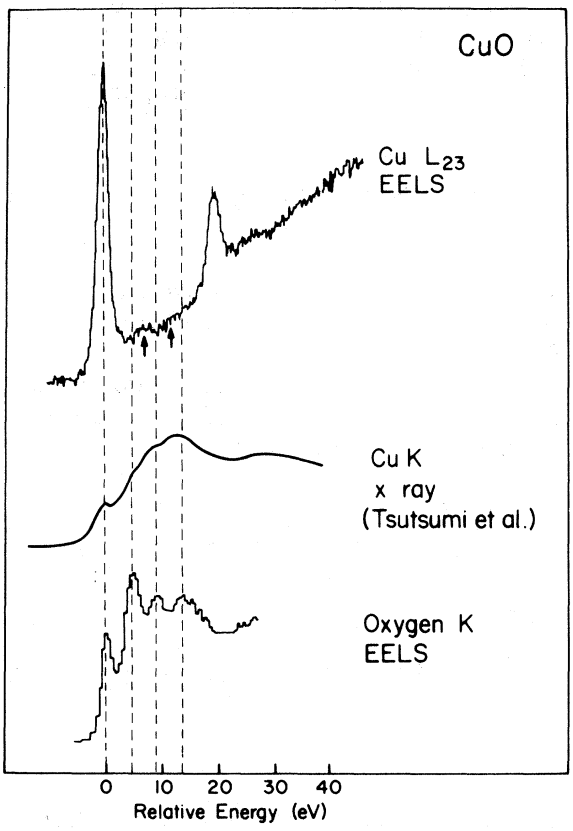

FIG. 4. Attempted alignment of fine-structure peaks in the same three core edges for CuO. (Fine structure above the Cu L_{23} edge is obscured above 20 eV by L_2-edge onset.) Lack of agreement signals the failure of the MO picture for interpreting these spectra.

What has been neglected? To begin, with the exception of TiO_2, all the oxides considered herein are antiferromagnetic insulators. Spin interactions associated with the electron configurations including the core hole can cause magnetic energy-level splittings of comparable magnitude to the ligand-field splittings assumed in the above MO picture.[38] Further, in insulators, insufficient screening of the core hole can give rise to excitonic effects, sometimes creating additional spectral peaks at energies below the onset of single-electron transitions.[39] It is not possible to deduce solely from experimental data how such effects would modify core-edge fine structure derived from densities of states with different symmetries.

To date, all interpretation of our core-edge spectra has been empirically based on a symmetry-determined model without the aid of calculation. This model has been shown to be clearly inadequate in at least some cases. In order to better understand our observed core-edge fine structure, we must consider more rigorous theoretical approaches. Two examples will be illustrated in the following sections. First, a nonmagnetic extended Hückel tight-binding band calculated for TiO_2 is undertaken (C.N.W. and R.H.) and a density of states calculated for comparison to the core-edge data. As expected, the calculation produces a broadened version of the MO picture. The neglect of the core hole is apparently justified by the good match between the DOS peaks and the experimental fine structure. Next we turn to a spin-polarized unrestricted Hartree-Fock band-structure computation for NiO (A.B.K.). In addition to a calculation of the OK-edge single-electron transition spectrum (core hole neglected), a cluster calculation of the allowed core exciton series is described. The initial peaks in the OK spectrum of NiO are identified as excitons, and their energies accurately predicted.

B. Band calculation for TiO_2

1. Method

The extended Hückel tight-binding method[40] is used to calculate the band structure for rutile TiO_2. After a brief outline of the general method (Sec. III B 1), we apply it to the case of TiO_2 to derive a band structure and DOS (Sec. III B 2) which we then compare to experiment (Sec. III B 3).

Given a set of atomic basis orbitals (χ_μ) for the atoms of the unit cell, the set of Bloch basis orbitals $[b_\mu(\vec{k})]$ is formed:

$$b_\mu(\vec{k})=N^{-1/2}\sum_l e^{i\vec{k}\cdot\vec{R}_l}\chi_\mu(\vec{r}-\vec{R}_l)\ , \tag{5}$$

where $\vec{k}$ is the wave vector, and the summation over l indicates a sum over direct lattice vectors. The tight-binding method involves an eigenvalue equation:

$$H(\vec{k})C(\vec{k})=S(\vec{k})C(\vec{k})\epsilon(\vec{k})\ , \tag{6}$$

where

$$H_{\mu\nu}(\vec{k})=\langle b_\mu(\vec{k})\,|\,H\,|\,b_\nu(\vec{k})\rangle \tag{7}$$

and

$$S_{\mu\nu}(\vec{k})=\langle b_\mu(\vec{k})\,|\,b_\nu(\vec{k})\rangle\ . \tag{8}$$

In the extended Hückel method the matrix elements of H are assumed to be

$$H_{ij}=K\frac{S_{ij}}{2}(H_{ii}+H_{jj})\ , \tag{9}$$

where H_{ii} is the orbital energy of the ith orbital, S_{ij} is the overlap between the ith and jth orbital, and K is a constant of parametrization.[41]

The solution of the eigenvalue problem, Eq. (6), yields the LCAO (linear combination of atomic orbitals) crystal orbitals $[\psi_n(\vec{k})]$,

$$\psi_n(\vec{k})=\sum_\mu C_{\mu n}(\vec{k})b_\mu(\vec{k})\ , \tag{10}$$

and eigenvalues $[\epsilon_n(\vec{k})]$. The band structure is then determined by repeating the above calculation for various values of $\vec{k}$.

Differentiating the eigenvalue equation and applying the normalization condition yields an expression for the $\vec{k}$ gradients[42–44]:

$$\frac{\partial\epsilon_n(\vec{k})}{\partial\vec{k}}=C_n^\dagger(\vec{k})D(\vec{k})C_n(\vec{k})\ , \tag{11}$$

where

$$D_{\mu\nu}(\vec{k})=i\sum_{\vec{R}}\{\epsilon^{i\vec{k}\cdot\vec{R}}[H_{\mu\nu}(\vec{R})-\epsilon_n(\vec{k})S_{\mu\nu}(\vec{R})]\}\vec{R}\ . \tag{12}$$

The bands are then plotted using the calculated set of energy eigenvalues and gradients. Interpolation between $\vec{k}$ points is carried out using the method of Kertész and Hughbanks.[45] Both the band energies and the DOS histogram are obtained from this interpolant.

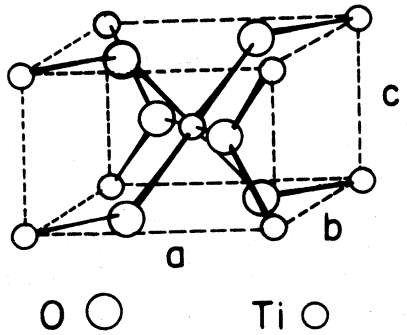

FIG. 5. Unit cell of the rutile form of TiO_2 ($a=b=4.5929$ Å, $c=2.9591$ Å).

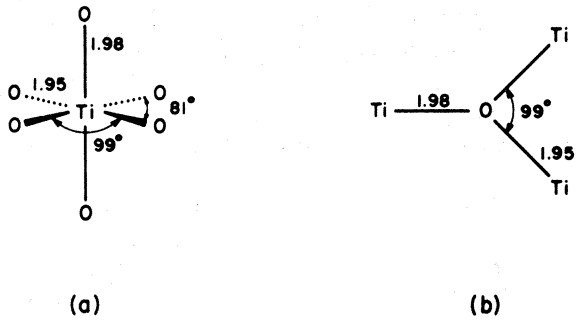

FIG. 6. Local environment (nearest neighbors) of Ti and O in the extended structure of TiO_2. In (a) the four equatorial oxygens lie in a plane perpendicular to the two axial oxygens. In (b) all atoms lie in the same plane.

2. *Crystal and band orbitals for TiO_2*

The rutile form of TiO_2 crystallizes in a tetragonal lattice belonging to the space group $P4_{2mnm}$. The atoms of the unit cell are shown in Fig. 5; the local environment of the Ti and O atoms are shown in Fig. 6. The oxygen atoms are seen to be arranged in a distorted octahedron around the titanium atom. The D_{2h} distortion from perpendicular bond angles and equal bond distances is relatively insignificant; our cluster calculations for $(TiO_2)^{8-}$ show that the distorted orbital energies never vary from the undistorted energies by more than 0.1 eV. Hence the assumption of perfect octahedral coordination of the Ti atom used in Sec. III A to generate the empirical molecular-orbital energy-level diagram shown in Fig. 2 appears reasonable. For convenience, we shall retain these octahedral symmetry labels to describe the orbitals in the rutile structure.

In order to estimate the relative charge densities of the various orbitals at the Ti or O atoms, a molecular-orbital calculation was performed on $(TiO_6)^{8-}$ in a perfect octahedral geometry, using the valence orbitals (Ti $3d$, $4s$, $4p$; O $2s$, $2p$). The resulting molecular orbitals segregate into five groups as expected from simple ligand-field arguments (see Fig. 2). Lowest in energy are the six O $2s$ bonding orbitals containing only 8—13 % Ti

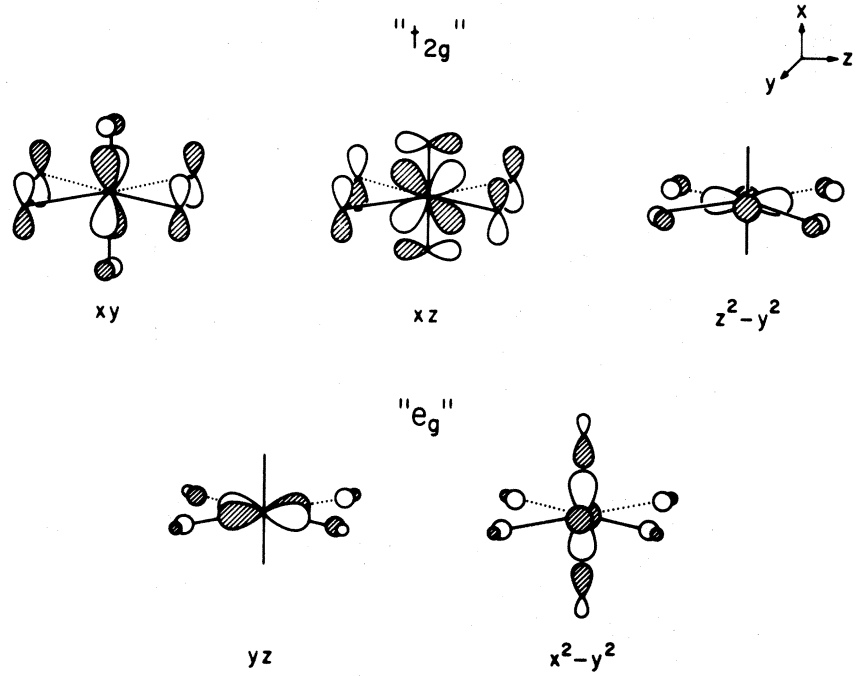

FIG. 7. MO's of TiO_6^{8-}. The t_{2g} orbitals are metal-oxygen π antibonding and lower in energy than the e_g orbitals which are metal-oxygen σ antibonding.

probability density.[46] Next the 18 O $2p$ orbitals segregate into six $O_{p\sigma}$ orbitals, whose density lobes point toward the metal, and 12 $O_{p\pi}$ orbitals whose lobes point perpendicular. These 18 orbitals are bonding between the O (80–100%) and the Ti (0–20%). Higher in energy are the metal d orbitals which are antibonding with the oxygens. These are mainly metal (~80%) and are labeled "t_{2g}" (π antibonding) and "e_g" (σ antibonding) (Fig. 7). The metal s and p orbitals (~90% metal) are very high in energy and are all unoccupied.

The orbitals of Ti in solid TiO_2 have similar bonding characteristics to those of the TiO_6^{8-}. There are two Ti and four O atoms per unit cell. The metal d-band orbitals at $\vec{k}=0$ for solid TiO_2 are shown in Fig. 8. Orbitals 17–22 are composed of metal d orbitals which point between the oxygen atoms and are therefore t_{2g} derived. Orbitals 23–26 are composed of those metal d orbitals which point toward the oxygen atoms and are therefore e_g derived. Comparing these crystal orbitals (Fig. 8) with the molecular orbitals (Fig. 7) we see that the t_{2g} orbitals 17 and 18 are metal–metal bonding and antibonding linear combinations of the d_{yz} and $d_{x^2-y^2}$ orbitals, 19 and 22 are like combinations of $d_{z^2-y^2}$, and 20 and 21 are like combinations of d_{xz} and d_{xy}. For the e_g orbitals, 23 and 24 are linear combinations of the metal–metal orbitals d_{xz} and d_{xy}, which are orthogonal to the t_{2g} orbitals above, while 25 and 26 are like combinations of the d_{yz} and $d_{x^2-y^2}$ orbitals.

The Brillouin zone of tetragonal TiO_2 is shown

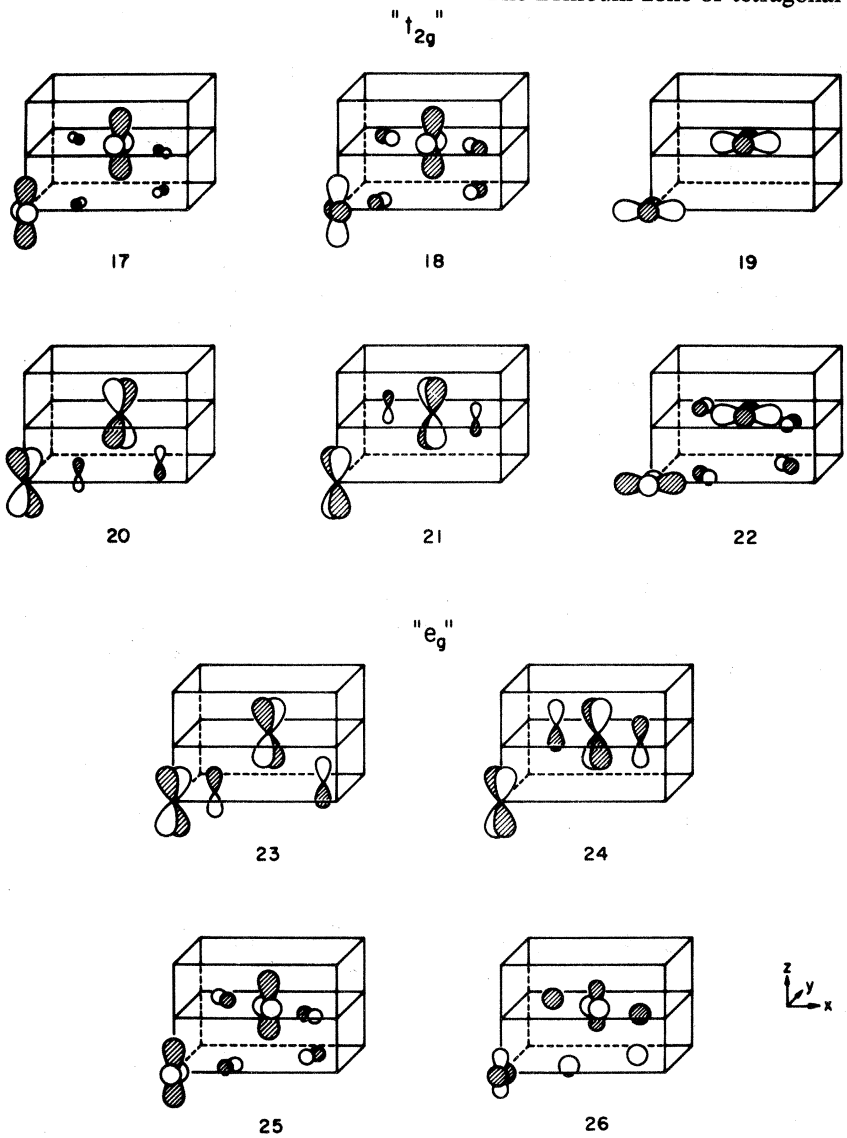

FIG. 8. Band orbitals of TiO_2 at $\vec{k}=0$. The orbitals again separate into t_{2g} and e_g groups.

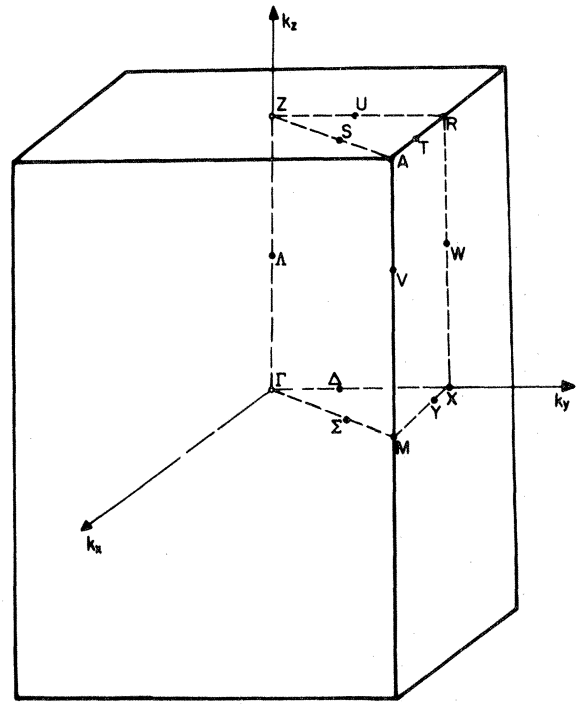

FIG. 9. Brillouin zone for a primitive tetragonal lattice (appropriate for the rutile TiO_2 structure).

in Fig. 9 and the calculated bands and DOS are shown in Fig. 10,[47] in which the energy-scale zero is arbitrary. The summation over direct lattice vectors in Eq. (5) was truncated by neglecting the matrix elements for atoms separated by more than 7.48 Å. Hence three shells of Ti-Ti interactions were included in the calculation. Since this calculation also includes only the valence orbitals, the resulting band structure again separates into five bands. Lowest in energy is a narrow band (~ -33 eV) not shown, composed mainly of the oxygen $2s$ (>90% O). Next up in energy (~ -16 eV) is a band corresponding to the filled $O_{p\sigma}$ ($2t_{1u}$) and $O_{p\pi}$ ($3t_{1u}$) orbitals (70–100% O; 0–30% Ti depending on the specific band energy and k point evaluated) and the two shaded peaks in the DOS (Fig. 10) may be thought of as a broadened overlapping version of the corresponding molecular-orbital levels (Fig. 2). The middle band in Fig. 10 (~ -10 eV) corresponds to the Ti d_{π^*} (t_{2g}) orbitals (55–95% Ti; 5–45% O), while the highest band corresponds to the Ti d_{σ^*} (e_g) orbitals (plus significant amounts of Ti $4s$ character) (60–70% Ti; 30–40% O). These last two bands are unoccupied, the Fermi level residing in the center of the band gap between the valence (shaded DOS) and conduction bands.

3. Comparison to experiment

We turn now to a comparison of theory with experiment. The band DOS has been redrawn at the top of Fig. 3 and aligned to the various symmetry-edge data from which the MO level spacings were deduced (Sec. II). Since the theoretical energies are not absolute, we compare only the energy spacings of the DOS with those of the related spectral peaks.

The calculated splitting of the occupied $O_{p\sigma}$ and $O_{p\pi}$ DOS maxima of 1.1 eV is a bit smaller than the experimental value (~ 1.7 eV) as determined from Tsutsumi's Ti K x-ray emission spectrum[30] also shown in Fig. 3. Hence the dashed lines running through the two x-ray peaks at ~ -6 and ~ -8 eV straddle the $O_{p\sigma}$ and $O_{p\pi}$ peaks in the DOS curve.

For the purpose of comparison, the band gap between the valence $O_{p\pi}$ and conduction Ti d_{π^*} bands is not drawn to scale. However, our theoretical value of 2.8 eV agrees reasonably well with various measured values[48] (3.0–3.3 eV) for the band gap. The calculated splitting of the Ti d_{π^*} and Ti d_{σ^*} band DOS maxima of 3.8 eV is a bit wider than the experimental peak spacings interpreted as being the $2t_{2g}-3e_g$ molecular-orbital-level splitting [Table III(a)]. We measure a spacing of 2.5 eV from our EELS Ti L_3 and O K data, while Tsutsumi's Ti K-edge data show a splitting of ~ 3 eV. (An earlier measurement by Fischer[23] of 2.1 eV is also smaller than the calculated band DOS splitting.) The dashed lines drawn through the two lowest-energy EELS peaks (Fig. 3) thus fall inside the calculated DOS maxima, although the agreement is close enough for us to state with confidence that the spectral features observed are indeed caused by this final-state ligand-field splitting.[49] Further confirmation of this interpretation comes from a more extensive augmented plane-wave (APW) calculation by Mattheiss[50] for RuO_2 showing two peaks in the unfilled p-projected DOS spaced by 3.4 eV. If this separation is scaled by the ratio of the RuO_2 (6.1 eV) to TiO_2 (4.6 eV) d bandwidths, then it suggests a spectral peak separation of 2.6 eV (Ref. 50) close to our measured EELS value of 2.5 eV.

The extended Hückel method does not include spin. Rather, the energy levels are calculated, and each is filled by two electrons (spin up and down). For nonmagnetic systems such as TiO_2, this is not a severe restriction. However, when we attempt to apply this same technique to the antiferromagnet NiO, metallic behavior due to a partially filled $3d$

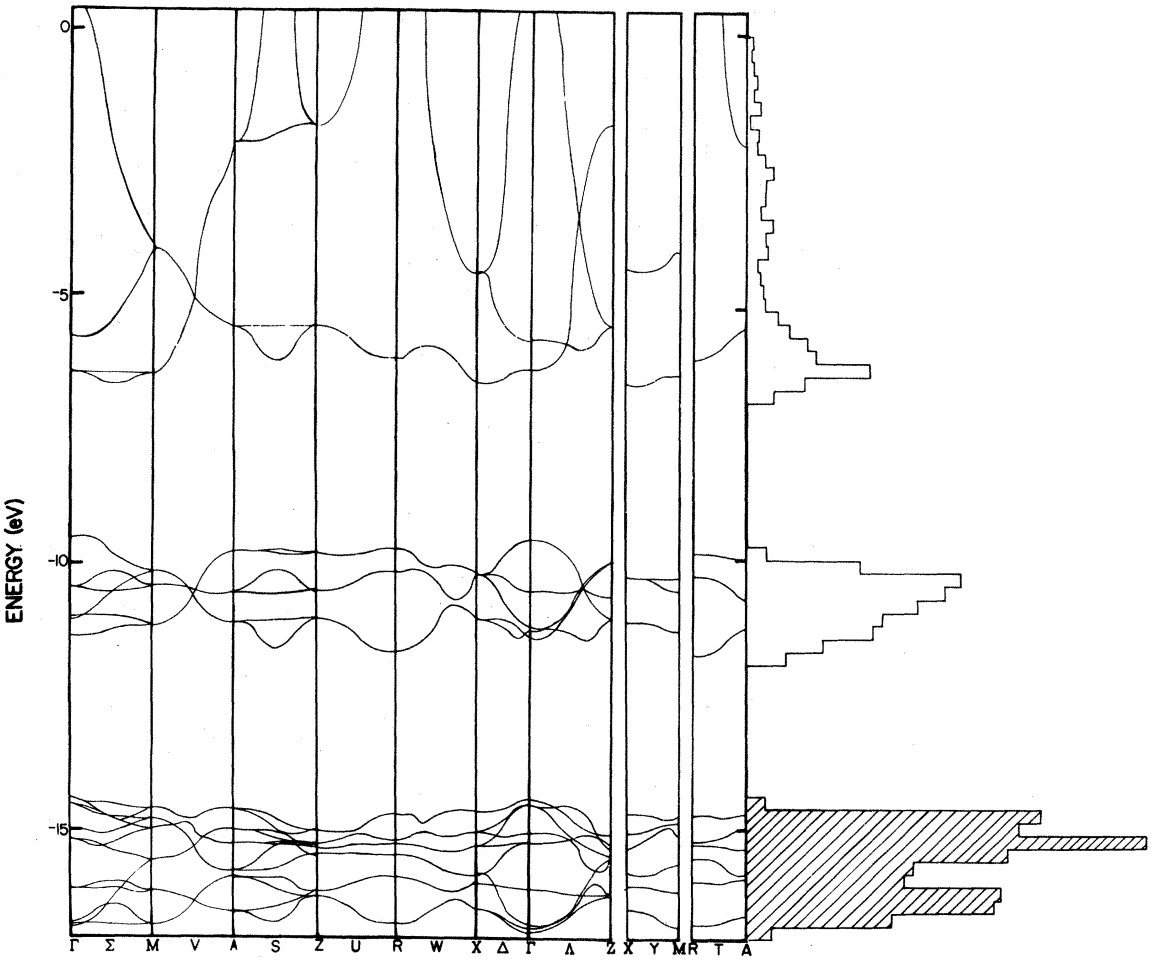

FIG. 10. Extended Hückel band structure and density of states for TiO_2.

band is erroneously predicted, and the calculated DOS bears no relation to data from any of the experimental probes of the occupied or unoccupied bands. Further, no account is taken of the unscreened core hole created in XAS or EELS, an effect which can produce gross changes in the spectrum at threshold. We conclude that more sophisticated calculations are required and this is illustrated for the case of NiO in the following section.

C. NiO calculation

The partially filled $3d$ bands found in Cr_2O_3, FeO, NiO, and CuO (and many other $3d$ transition metal oxides) give rise to magnetic effects. We consider here the case of NiO, which has a Néel temperature of about 525 K, below which it is an antiferromagnet.[51] On the basis of elementary band theory, one would expect NiO to exhibit metallic behavior, since only eight out of ten d orbitals are filled. Instead, it is strongly insulating, with a measured band gap of ~ 4 eV.[52] Previous *ab initio* band calculations for NiO[53–56] have failed to predict the wide-gap insulating and magnetic properties observed. A new calculation for the electonic structure of NiO has been completed (A.B.K.) which gives reasonable agreement with photoemission probes of the occupied levels, and this has been described in detail elsewhere.[57,58] We present here a brief synopsis of the method and also a comparison of theory to the EELS data presented above.

First we define the physics behind the energy band. We use here the one common to Hartree-Fock theories. The occupied energy levels refer to the negative of the energy needed to remove an electron from the system (ionization potentials), whereas the virtual ones are the negative of the energy gained in adding an electron to the system (electron affinities). In this study the Hartree-Fock problem is solved separately to a high degree of ac-

curacy for each state in question, and total-energy differences then define the bands. The basic method used here is the self-consistent Hartree-Fock method in its fully unrestricted form (UHF). In this method one describes the n-electron wave function for the system as an antisymmetrized product of one-electron orbitals. That is

$$\psi_\alpha(\vec{x}_1 \cdots \vec{x}_n) \simeq (n!)^{-1/2} \det || \phi_i^\alpha(\vec{x}_j) || \ . \tag{13}$$

Here $\vec{x}_i$ is the ith electron coordinate and includes both space and spin dependence. The one-electron orbitals ϕ_i are constrained to be orthonormal and to be eigenstates of s_z. No further constraints are imposed upon ϕ other than that they minimize the expectation value of the n-electron Hamiltonian with respect to our functional form for ψ. This yields the canonical UHF equation for determining the ϕ's:

$$F^\alpha(\rho^\alpha)\phi_i^\alpha(\vec{x}) = \epsilon_i^\alpha \phi_i^\alpha(\vec{x}) \ , \tag{14}$$

where

$$\rho^\alpha(\vec{x}\vec{x}^{\,1}) = \sum_{i=1}^{n} \phi_i^\alpha(\vec{x}) \phi_i^{\alpha+}(\vec{x}^{\,1}) \tag{15}$$

and

$$F(\rho^\alpha) = -\frac{\hbar^2}{2m}\nabla^2 - \sum_{I=1}^{N} \frac{Z_I e^2}{|\vec{r}-\vec{R}_I|} + e^2 \int \frac{\rho^\alpha(\vec{x}^{\,1}\vec{x}^{\,1})}{|\vec{r}-\vec{r}^{\,1}|} d\vec{x}^{\,1} - e^2 \rho^\alpha(\vec{x}\vec{x}^{\,1}) / |\vec{r}-\vec{r}^{\,1}| P \ , \tag{16}$$

and P is the operator which interchanges coordinates $\vec{x}$ and $\vec{x}^{\,1}$. E_α is then the energy of state ψ_α:

$$E_\alpha = \langle \Psi_\alpha | H | \Psi_\alpha \rangle = E_\alpha(\rho^\alpha) \ . \tag{17}$$

Because NiO possesses both broad and narrow bands, we find it necessary to use two different schemes for dealing with the hole left behind in removing the electron whose energy we wish to compute. In the narrow-band case of the Ni $3d$ levels, we describe the hole by a valence bond (VB) scheme and remove an orbital $\phi_i(\vec{x}-\vec{R}_I)$ localized on ion site $\vec{R}_I$, leaving a hole of unit charge on site I. In the broad-band case of O $2p$ level and the $4s$ part of the conduction band, we remove a nonlocal Bloch orbital made up of a linear combination of the $\vec{\phi}_i(\vec{x}-\vec{R}_i)$. This differentiation gives rise to a considerable band gap in the $3d$ states which is absent from conventional band models.

Finally, we note that the presence of a local hole is not acceptable as a final model in that the translational symmetry of the Hamiltonian requires the many-body wave function ψ_α be periodic. So, for the VB case, we symmetry project Bloch sums of the VB many-electron trial function in order to regain translational symmetry. This results in a broadening of the conduction Ni $3d$ levels and hybridization of the Ni $3d$ and O $2p$ bands.

The combined VB band structure is shown in Fig. 11, along with the density of states curve. A computed band gap of 4.8 eV compares with the optically measured gap of 4 eV.[52] The two large peaks in the conduction band DOS are associated with the flat portions of the mostly Ni $3d$ band.

We now calculate the O K-edge energy-loss spectrum ($\epsilon_2(E) \simeq \mathrm{Im}[-1/\epsilon(E)]$, where $\epsilon(E)$ is the dielectric function) from the above band structure; both the transition intensity and the associated absolute energy are determined. Figure 12 matches up the theoretical results with experiment. The band single-particle transition strength is shown as the solid curve running along the bottom of the figure. Above 555 eV, the calculation may be unreliable due to basis-set limitations.

The four spikes sticking up from the $\epsilon_2(E)$

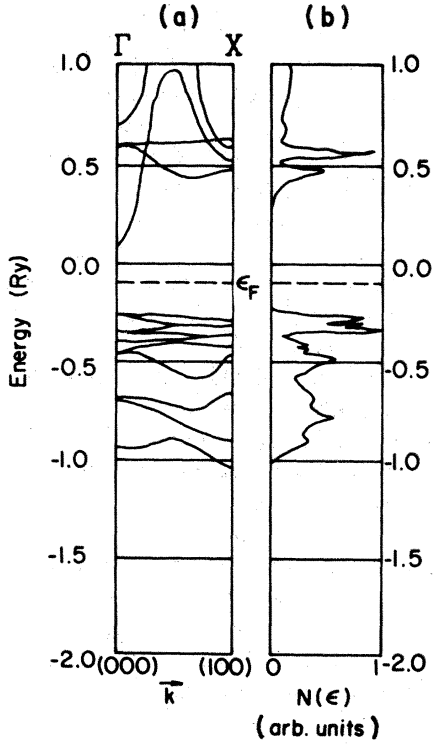

FIG. 11. Calculated UHF band structure (a) and density of states (b) for NiO. The Fermi level is shown as a dashed line.

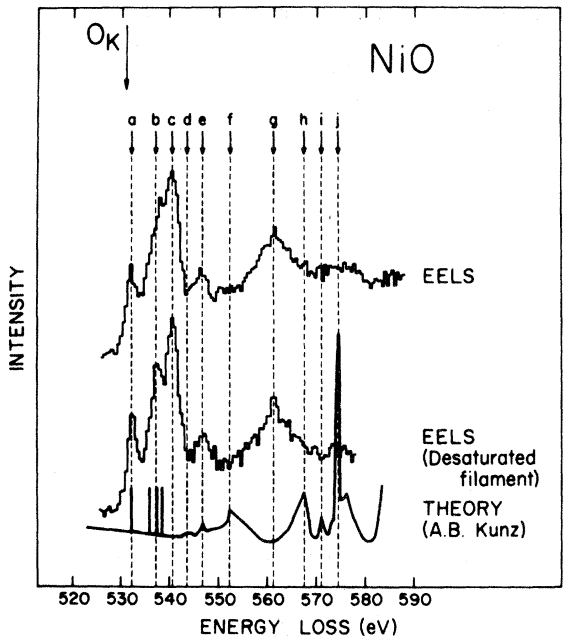

FIG. 12. Calculated and measured O K spectra in NiO.

theory curve are the allowed Frenkel core excitons which are also calculated by solving Eq. (14) using an updated version of the UHF method.[59] Here, however, we calculate the allowed transitions localized on a particular oxygen atom. The NiO solid is approximated by a Ni_6O cluster imbedded in a charge neutral $5\times5\times5$ array of point ions chosen self-consistently to simulate the remainder of the solid. In the region of interest the ionic potential has an accuracy of better than 0.25 eV. The method of separating out this bounding potential and incorporating its effect into the total-energy calculation is described in the literature and need not be considered here.[60]

In performing these studies a Gaussian set of double-zeta accuracy is used for Ni^{2+} and contracted to a minimal set chosen for the NiO crystal. For the O^{2-} a Gaussian set of double-zeta accuracy plus several s and p polarization functions were used in an uncontracted form. Self-consistent calculations were performed for the Ni_6O cluster for O^{2-} in the states $1s^2\,2s^2 2p^6$ (ground state), $1s\,2s^2 2p^6$ (ionization limit), $1s\,2s^2 2p^6 3s$ (first-excited state), $1s\,2s^2 2p^6 3p$ (second-excited state). The results are that the ionization limit is 539 eV, the first excitation is at 532 eV, and the second excitation is at 536 eV. Due to the trigonal distortion of NiO from perfect fcc the first excitation becomes somewhat allowed. Variational collapse prevents self-consistent determination of the excitation to $4p$ or $5p$. However, we can use the orthogonal atomic operator (OAO) method to determine these approximately.[61] These are predicted to lie at 537.5 and 538.5 eV, respectively.

Before continuing, we comment upon the expected theoretical accuracy of the UHF method for such x-ray edge studies. Systems isoelectronic to O^{2-} have been studied, in particular, the K edges of CH_4 and Ne.[62] For CH_4 the $1s$ ionization potential (IP) is found to be 290.58 eV by this technique as compared to 290.6 eV in experiment. The theoretical value of the first excitation from the $1s$ shell is 288.5 eV and experiment is 288.3 eV. In the case of Ne, theory predicts 870.27 eV against an experimental value of 870.1 eV for the $1s$ IP. As seen here, there is no reason to expect these calculations to have any significant inaccuracies. Furthermore, recent detailed studies using these exact techniques on Li and Na halides indicate that accuracies of 0.5 eV are easily possible for solid-state situations.[63] It is speculated that some of this accuracy is fortuitous in that atomic correlation effects would increase the gaps and solid-state ones compress the gaps and hence one has compensating errors. Nonetheless, one can estimate these effects to have a size of 1 eV for these systems and hence even at worst the numbers reported here should have better than 1-eV accuracy. For O^{2-} relativistic effects are not significant.

Returning now to Fig. 12, we compare the theoretical core exciton plus band $\epsilon_2(E)$ curve with the experimental data. In the lower EELS curve, the data was obtained at better energy resolution but poorer counting statistics than for the top curve. We see that the computed energy of the first core exciton (a) at 532 eV is in very good agreement with the position of the first spectral peak. The next three excitons then blur into the observed EELS peak (b) centered at 537.5 eV. Since the ionization potential is calculated to be 539 eV, the large EELS peak (c) at 540.5 eV is attributed to a mixture of the band edge enhanced by electron-hole interaction and further series limit excitons.[64]

The two large DOS peaks centered at about 0.5 Ry in Fig. 11 arise from bands with mostly d character. The dipole matrix element with the O $1s$ level as the initial state greatly reduces the transition strength to these Ni d bands, and the resulting peaks (d,e) in the ϵ_2 curve in Fig. 12 are quite small. Peak e fits the EELS spectral peak at 547 eV, while the lack of any EELS feature matching hump d in the ϵ_2 curve is not surprising considering its small size. While peak f in the ϵ_2 curve

may correspond to the slight rise in the top EELS curve, the prominent broad peak (g) displayed by both EELS curves is plainly absent from the calculation. As previously mentioned, the band $\epsilon_2(E)$ curve is not reliable above 555 eV due to basis set limitations, and so the apparent mismatch of theory to experiment in this energy region was to be expected. The calculation does accurately predict the energies of the initial EELS spectral fine structure, and shows that core excitons and not peaks in the conduction-band DOS are responsible for the sharp peaks at onset. This repudiates our earlier guess that the peak(s) $b(b')$ observed in all the $3d$ transition oxide OK edges shown in Fig. 1 represented transitions to a narrowing metal d-band DOS. Core excitons may well play a role in determining the fine structure at onset in some of the rest of these spectra. Their appearance would explain the observed absence of correlation between peaks in near-edge structure evinced in the metal K and L and the OK edges (as was shown in Fig. 4 for CuO) since the excitonic binding energies are not expected to be the same. Conversely, we may interpret the agreement between the three core-edge fine structures in TiO_2 (Fig. 3) as evidence that core excitons are not observed in this case.

Under what conditions may one expect exciton effects to be prominent, i.e., why does NiO show exciton effects when TiO_2 does not? We have some ideas on this point, although they are only educated speculation. A fundamental difference between NiO and TiO_2 is that NiO is best described as an ionic solid while TiO_2 is more covalent. The occupied states in NiO are well represented by relatively local orbitals on a Ni or O sublattice ($\langle r\rangle_{\mathrm{Ni}\,3d}=0.95$ a.u. and $\langle r\rangle_{\mathrm{O}\,2p}=1.65$ a.u. compared to the lattice constant of 7.92 a.u.). Thus the exciton's electron orbital can easily be made orthogonal to the occupied orbitals, have its energy minimized, and still be quite compact. TiO_2 is, however, another matter. Because the system is covalent any attempt at a true rotation into orbitals localized on Ti or O cannot span just the occupied space but must also include the low-lying antibonding part of the conduction band as well. Therefore, the true occupied wave functions are not local but rather covalent, bonding-type orbitals, shared jointly by Ti and O. Consequently, orthogonality of the exciton's electron state forces the exciton into a rather diffuse orbital. Furthermore, there are lower-lying virtual *band* states built up of the antibonding parts of the local orbitals present in TiO_2 which are absent in NiO. The change of radius means the exciton in TiO_2 sees more of the lattice than in NiO and hence has its binding energy (BE) reduced by the dielectric screening ($\mathrm{BE}\alpha 1/\epsilon^2$) much more severely than does the electron in NiO. In the latter case, the exciton, being more compact, is screened by an effective dielectric constant which should be far less than that of the crystal. The secondary effect of the low-lying TiO_2 antibonding bands is to further increase the dielectric constant of TiO_2 over that of the ionic cases. Thus we expect TiO_2 to be like Si in which the excitons are bound by millivolts[65] rather than like NiO or the alkali halides,[66] where excitons are bound by volts.

IV. SUMMARY

We have presented data on the 1s subshell excitation in oxides of half the $3d$ transition metals, the first such study to be carried out using fast electron scattering, and the first systematic study across the row by either EELS or x-ray absorption. The multipeaked structure observed near onset in these edges is found to vary markedly between the different oxides. Other measurements by complementary techniques yield results in good agreement with ours, although nonlinearities resulting from the various indirect measurement techniques employed cause variation in the spectral shapes and peak intensities. An empirical symmetry-based molecular-orbital model has been invoked in an attempt to interpret the data. Comparisons are made to the fine structure evinced in the metal K and L_3 edges in these same oxides in an attempt to verify the consistency of the MO model energy-level spacings. While the three symmetry edges of TiO_2 display structure consistent with this model, it fails for at least some of the other oxides studied.

Finding our empirical interpretation scheme to be insufficient, we turn to more rigorous theoretical approaches. First, an extended Hückel tight-binding calculation for the band structure of TiO_2 has been described including comparison of the crystal orbital to the $(TiO_6)^{8-}$ cluster molecular orbitals. We show that the valence orbitals in solid TiO_2 have similar bonding characteristics to those in $(TiO_6)^{8-}$. As expected, the density of states for solid TiO_2 displays peaks which correspond to broadened, overlapping versions of the MO energy levels. We find that the separation of the first two unoccupied-band DOS peaks is in reasonable agreement with the experimental separation of the first two fine-structure peaks in the OK, TiK, and

Ti L_{23} edges, providing corroboration for our MO interpretation of the core-edge spectra of TiO_2.

A self-consistent Hartree-Fock calculation for the energy bands of antiferromagnetic NiO has been presented. A hybrid valence-bond—band scheme is employed in order to differentiate between the narrow Ni 3*d* band and the other valence bands which are broad in energy, and this gives rise to a considerable band gap in the 3*d* states absent from previous calculations. Next, we compute both the O *K*-edge single-particle transition strength (core-hole neglected) and also the allowed core exciton series. The energies of the initial spectral peaks are accurately predicted and these are shown to be core excitons and not peaks in the conduction-band DOS. This result not only repudiates our initial MO interpretation of the data, but also shows the usual assumption that near-edge structure is related to the unoccupied density of states of the initial solid (before core-hole excitation) to be incorrect for NiO. Core excitons may well play a role in the spectra of others of the oxides presented here, and this would explain the observed lack of correlation between peaks in the near-edge structure for different atoms in the same solid.

ACKNOWLEDGMENTS

We wish to thank Professor J. Silcox, Dr. B. Mattheiss, Professor S. T. Manson, and Sunil Wijeyesekera for helpful discussions and communications. We are especially grateful to Professor K. Tsutsumi for providing us with his unpublished data for the metal *K*-edge x-ray-absorption spectra of the 3*d* transition-metal oxides and to T. Hughbanks for a critical reading of the manuscript. The comments of the referee were particularly helpful. Financial support is gratefully acknowledged from the National Science Foundation through the Cornell Materials Science Center, Grant Nos. DMR-79-24008 (L.A.G. and R.D.L.), DMR-76-81083 (C.N.W. and R.H.); and through DMR-77-23999 (A.B.K.).

---

*Present address: Biomedical Engineering and Instrumentation Branch, Building 13, Room 3W13, National Institutes of Health, Bethesda, Maryland 20205.

[1]F. W. Lytle, in *Advances in X-ray Analysis,* edited by G. R. Mallett, M. Fay, and W. M. Mueller (Plenum, New York, 1966), p. 398.

[2]D. E. Sayers, E. A. Stern, and F. W. Lytle, Phys. Rev. Lett. 27, 1024 (1971).

[3]E. A. Stern, Phys. Rev. B 10, 3027 (1974).

[4]F. W. Lytle, D. E. Sayers, and E. A. Stern, Phys. Rev. B 11, 4825 (1975).

[5]E. A. Stern, D. E. Sayers, and F. W. Lytle, Phys. Rev. B 11, 4836 (1975).

[6]R. D. Leapman, L. A. Grunes, P. L. Fejes, and J. Silcox, in *EXAFS Spectroscopy: Techniques and Applications,* edited by B. K. Teo and D. C. Joy (Plenum, New York, 1981), p. 217.

[7]S. Csillag, D. E. Johnson, and E. A. Stern, in *EXAFS Spectroscopy: Techniques and Applications,* edited by B. K. Teo and D. C. Joy (Plenum, New York, 1981).

[8]C. R. Natoli, D. K. Misemer, and S. Doniach, Phys. Rev. A 22, 1104 (1980).

[9]R. A. Bair and W. A. Goddard, Phys. Rev. B 22, 2767 (1980).

[10]U. Fano and J. W. Cooper, Rev. Mod. Phys. 40, 441 (1968).

[11]H. A. Bethe, Ann. Phys. (Leipzig) 5, 325 (1930).

[12]L. A. Grunes and R. D. Leapman, Phys. Rev. B 22, 3778 (1980).

[13]M. Inokuti, Rev. Mod. Phys. 43, 297 (1971).

[14]L. V. Azaroff and D. M. Pease, in *X-ray Spectroscopy,* edited by L. V. Azaroff (McGraw-Hill, New York, 1974).

[15]J. E. Müller, Ph.D. thesis, Cornell University, 1980 (unpublished).

[16]D. J. Nagel, D. A. Papaconstantopoulos, J. W. McCaffrey, and J. W. Criss, *Proceedings of the International Symposium on X-ray Spectra and Electronic Structure of Matter,* edited by A Faessler and C. Wiech (Academic, New York, 1973), p. 51.

[17]G. H. Curtis and J. Silcox, Rev. Sci. Instrum. 42, 630 (1971).

[18]P. E. Batson, Ph.D. thesis, Cornell University, 1976 (unpublished).

[19]B. Watkins and P. L. Fejes, Cornell University Materials Science Center Report No. 3082 (unpublished).

[20]*Powder Diffraction File* (JCPDS—International Centre for Diffraction Data, Swarthmore, Penn., 1980).

[21]S. T. Manson and M. Inokuti, J. Phys. B 13, L323 (1980); and private communication.

[22]R. D. Leapman, L. A. Grunes, and P. L. Fejes, Phys. Rev. B (in press).

[23]D. W. Fischer, Phys. Rev. B 5, 4219 (1972).

[24]D. W. Fischer, J. Phys. Chem. Solids 32, 2455 (1971).

[25]J. Stöhr, R. Jaeger, J. Feldhaus, S. Brennan, D. Norman, and G. Apai, Appl. Optics 19, 3911 (1980).

[26]D. J. Nagel and W. L. Baun, in *X-ray Spectroscopy,* edited by L. V. Azaroff (McGraw-Hill, New York, 1974). See especially Fig. 9-19.

[27]S. Anderson and C. Nyberg, Solid State Commun. 15, 1145 (1974).

[28]J. E. Houston and R. L. Park, J. Chem. Phys. 55,

4601 (1971).
[29]G. Ertl and K. Wandelt, Z. Naturforsch. 29A, 768 (1974).
[30]K. Tsutsumi, O. Aita, and K. Ichikawa, Phys. Rev. B 15, 4638 (1977).
[31]G. Albrecht, *Rontgenspectren und Chemische Bindung* (Karl Marx University, Leipzig, 1966), p. 3.
[32]A. Z. Menshikov and S. A. Nemnonov, Bull. Acad. Sci. USSR (Phys. Ser.) 27, 402 (1963).
[33]M. Belli, A. Scafati, A. Bianconi, S. Mobilio, L. Palladino, A. Reale, and E. Burattini, Solid State Commun. 35, 355 (1980).
[34]K. Ichikawa, O. Aita, H. Nakamori, M. Kamada, and K. Tsutsumi, Jpn. J. Appl. Phys. 17, Suppl. 17-2, 157 (1978).
[35]C. Sugiura and S. Nakai, Jpn. J. Appl. Phys. 17, Suppl. 17-2, 190 (1978).
[36]G. L. Glenn and C. G. Dodd, J. Appl. Phys. 39, 5372 (1968).
[37]K. Tsutsumi, private communication of unpublished results.
[38]J. A. Tossel, J. Electron. Spectrosc. Relat. Phenom. 8, 1 (1976).
[39]For example, E. E. Koch, C. Kunz, and B. Sonntag, Phys. Rep. 29, 153 (1977), and references therein.
[40]See, for example, J.-M. André, *Electronic Structure of Polymers and Molecular Crystals,* edited by J.-M. André and J. Ladik (Plenum, New York, 1974), p. 1; J. Ladik, *ibid.*, p. 23; M.-H. Whangbo and R. Hoffman, J. Am. Chem. Soc. 100, 6093 (1978).
[41]J. H. Ammeter, H.-B. Rurgi, J. C. Thibeault, and R. Hoffman, J. Am. Chem. Soc. 100, 3686 (1978).
[42]G. Del Ra, J. Ladik, and G. Biczo, Phys. Rev. 155, 997 (1967).
[43]J.-M. André and J. Dehalle, Chem. Phys. Lett. 17, 145 (1972).
[44]J. Dehalle, Ann. Soc. Sci. Bruxelles, Ser. 1, 86, 227 (1972).
[45]M. Kertész and T. Hughbanks, Phys. Rev. B 24, 6870 (1981).
[46]The projected probability density was calculated from a standard Mulliken population analysis; R. S. Mulliken, J. Chem. Phys. 23, 1833 (1955); 1841 (1955); 2338 (1955); 2342 (1955).
[47]The symmetries were assigned using the conventions given in S. C. Miller and W. F. Love, *Tables of Irreducible Representations of Space Groups and Co-representations of Magnetic Space Groups* (Pruett, Boulder, Colorado, 1967).
[48]W. H. Strehlow and E. L. Cook, J. Phys. Chem. Ref. Data 2, 163 (1973).
[49]The parameters chosen for this semiempirical calculation were those employed previously for molecular Ti complexes having similar environments to that found in TiO_2. Parameter variation to fit the experimental data was not carried out, since the agreement was sufficient for purposes of interpretation.
[50]L. F. Mattheiss, Phys. Rev. B 13, 2433 (1976), and private communication.
[51]R. Brandow, Int. J. Quantum Chem. Symp. 10, 417; Adv. Phys. 26, 651 (1977).
[52]R. J. Powell and W. E. Spicer, Phys. Rev. B 2, 2182 (1970).
[53]L. F. Matheiss, Phys. Rev. B 5, 290 (1972).
[54]T. M. Wilson, Int. J. Quantum Chem. Symp. 2, 269 (1968); 3, 757 (1970).
[55]T. C. Collins, A. B. Kunz, and J. Ivey, Int. J. Quantum Chem. Symp. 9, 487 (1975).
[56]A. B. Kunz and G. T. Suratt, Solid State Commun. 25, 9 (1978).
[57]A. B. Kunz, in *Excited States in Quantum Chemistry,* edited by C. A. Nicolaides and D. R. Beck (Reidel, Dordrecht, Holland, 1979).
[58]A. B. Kunz, J. Phys. C 14, L455 (1981).
[59]R. F. Marshall, R. J. Blint, and A. B. Kunz, Phys. Rev. B 13, 3333 (1976).
[60]A. B. Kunz and D. L. Klein, Phys. Rev. B 1, 4614 (1978).
[61]T. C. Collins, A. B. Kunz, and P. W. Deutsch, Phys. Rev. A 10, 1034 (1974).
[62]P. W. Deutsch and A. B. Kunz, J. Chem. Phys. 62, 4069 (1975).
[63]A. B. Kunz, J. C. Boisvert, and T. O. Woodruff (unpublished).
[64]We note that the theory predicts sufficient continuous absorption from higher edges underlying the 530–540 eV region to permit photo yield from these so-called core excitons. A.B.K. computes using band theory an underlying $\epsilon_2(E)$ of about 0.09 in this region. (See Fig. 12; the tall spike in the THEORY $\epsilon_2(E)$ curve reaches a peak value of 0.38.)
[65]F. C. Brown and O. P. Rustgi, Phys. Rev. Lett. 28, 497 (1972).
[66]S. T. Pantelides, Phys. Rev. B 11, 2391 (1975).